Eur. Phys. J. C 49, 181–186 (2007)
DOI 10.1140/epjc/s10052-006-0127-0

THE EUROPEAN PHYSICAL JOURNAL C

Regular Article – Theoretical Physics

Heavy quarks at RHIC from parton transport theory

D. Molnar[1,2,a]

[1] Physics Department, Purdue University, 525 Northwestern Ave, West Lafayette, IN 47907, USA
[2] RIKEN BNL Research Center, Upton, NY 11973-5000, USA

Received: 18 August 2006 /
Published online: 2 December 2006 – © Springer-Verlag / Società Italiana di Fisica 2006

Abstract. There are several indications that an opaque partonic medium is created in energetic Au + Au collisions ($\sqrt{s_{NN}} \sim 100$ GeV/nucleon) at the relativistic heavy ion collider (RHIC). At the extreme densities of $\sim$ 10–100 times normal nuclear density reached, even heavy-flavor hadrons are affected significantly. Heavy-quark observables are presented from the parton transport model MPC, focusing on the nuclear suppression pattern, azimuthal anisotropy ("elliptic flow"), and azimuthal correlations. Comparison with Au + Au data at top RHIC energy $\sqrt{s_{NN}} = 200$ GeV indicates significant heavy-quark rescattering, corresponding roughly five times higher opacities than estimates based on leading-order perturbative QCD. We propose measurements of charm–anticharm, e.g., D-meson azimuthal correlations as a sensitive, independent probe to corroborate these findings.

PACS. 25.75.-q; 25.75.Ld; 25.75.Gz

1 Introduction

Recent heavy-ion collision experiments at the relativistic heavy ion collider (RHIC) have generated a lot of excitement. Among the most remarkable discoveries are the large azimuthal momentum anisotropy ("elliptic flow") [1–3] and strong attenuation of particles with high transverse momentum created in the collision ("jet quenching") [4–7], which indicate the formation of extremely opaque quark–gluon matter that exhibits highly collective, near hydrodynamic behavior [8–10]. The mechanism of rapid randomization and the high degree of equilibration in the system is not yet understood. For example, it is puzzling that dissipative effects (such as viscosity) from nonequilibrim transport are significant [11] and yet ideal (nondissipative) hydrodynamics can describe the data quite well [12–15]. For heavy quarks, only partial equilibration is expected because collective effects are weaker due to the large mass. Therefore, heavy-flavor observables are of great interest as an orthogonal set of probes to gain more insight and cross-check dynamical scenarios.

There are two main dynamical frameworks to study heavy quarks in heavy-ion collisions: parton energy loss models [16–21] and transport approaches Energy loss models consider multiple parton scattering in the dense medium in an Eikonal approach (i.e., straight-line trajectories), applicable only for very large heavy-quark energies. The advantage, on the other hand, is that coherence effects are taken into account. For charm and bottom, small-angle gluon radiation, and therefore radiative energy loss, is suppressed relative to light quarks because of the large quark mass ("dead-cone" effect) [19, 20]. Surprisingly, recent data from RHIC[31–33] indicate little light–heavy difference in the high-p_{T} suppression pattern. Though the puzzle has not yet been resolved, it is clear now that elastic energy loss, previously neglected, plays an important role [21, 34] besides radiative energy loss.

Transport models, on the other hand, do not impose kinematic limitations but typically include incoherent, elastic interactions only. They are ideal tools to study equilibration because they have a hydrodynamic (local equilibrium) limit. The dynamics is formulated in terms of (on-shell) 6 + 1D phase-space distributions that obey the relativistic Boltzmann transport equation [22–25, 29, 30], and the results are mainly sensitive to the transport opacity of the system [23, 24]. In case particles undergo a lot of scatterings, the evolution for the bulk of the system (i.e., particles that come from "typical" scattering events and therefore are affected little by fluctuations in scattering angles or the number of scatterings) can be approximated with the Fokker–Planck equation [26–28].

In this work we report on heavy-flavor (charm and bottom) observables from covariant transport theory with elastic $2 \to 2$ interactions. The covariant transport solutions were obtained using the Molnar parton cascade (MPC) algorithm [25, 35]. Extending earlier results for charm quark elliptic flow (v_2) [36], we include bottom quarks and also study heavy nuclear suppression (R_{AA}) and charm–anticharm azimuthal correlations. The results are compared to the RHIC data and also other trans-

[a] e-mail: molnar@physics.purdue.edu

port calculations in the literature based on the (non-covariant) AMPT transport model [29] or the Fokker–Planck limit [28].

2 Covariant transport theory

We consider here the Lorentz-covariant parton transport theory in [22–25, 37, 38], in which the on-shell parton phase-space densities $\{f_i(x,\mathbf{p})\}$ evolve with elastic $2\to2$ rates as

$$p_1^\mu\partial_\mu f_{1,i} = \frac{1}{16\pi^2}\sum_j \int_2\int_3\int_4 (f_{3,i}f_{4,j}-f_{1,i}f_{2,j})\left|\bar{\mathcal{M}}^{ij\to ij}_{12\to34}\right|^2 \times\delta^4(p_1+p_2-p_3-p_4)+S_i(x,\mathbf{p}_1)\,. \quad (1)$$

Here $|\bar{\mathcal{M}}|^2$ is the polarization averaged scattering matrix element squared, the integrals are shorthands for $\int_a \equiv \int \mathrm{d}^3p_a/(2E_a)$, while $f_{a,i}\equiv f_i(x,\mathbf{p}_a)$. The source functions $\{S_i(x,\mathbf{p})\}$ specify the initial conditions.

Though (1) can be generalized for bosons and fermions, or inelastic $3\leftrightarrow2$ processes [30, 39], we for simplicity limit our study to a quadratic dependence of the collision integral on f.

We apply (1) to a system of massless gluons and light quarks/antiquarks ($q=u,d,s,\bar{u},\bar{d},\bar{s}$), and charm and bottom quarks/antiquarks with mass $m_c=1.5\,\mathrm{GeV}$, $m_b=4.75\,\mathrm{GeV}$. All elastic $2\to2$ QCD processes were taken into account: $gg\to gg$, $gQ\to gQ$, $QQ\to QQ$, and $QQ'\to QQ'$. Inelastic $2\to2$ processes, such as $gg\leftrightarrow Q\bar{Q}$, are straightforward to include [36] but were ignored here for faster simulations.

The transport solutions were obtained via the MPC algorithm [25, 35], which employs the parton subdivision technique [40] to maintain Lorentz covariance and causality. Acausal artifacts in the naive cascade approach (that uses no subdivision) are known to affect basic observables such as spectra, elliptic flow, and freezeout distributions in spacetime [23, 24, 38].

As in [22–24], only the most divergent parts of the matrix elements were considered, regulated using a Debye mass of $\mu_\mathrm{D}=0.7\,\mathrm{GeV}$. For perturbative QCD processes at leading order, *including* scatterings of heavy quarks with gluons and light quarks [41], we thus have

$$\frac{\mathrm{d}\sigma_{gg\to gg}}{\mathrm{d}t}\approx\frac{9}{4}\frac{\mathrm{d}\sigma_{gQ\to gQ}}{\mathrm{d}t}\approx\left(\frac{9}{4}\right)^2\frac{\mathrm{d}\sigma_{QQ'\to QQ'}}{\mathrm{d}t} =\frac{9\pi\alpha_s^2}{2(t-\mu_\mathrm{D}^2)^2}\left(1+\frac{\mu_\mathrm{D}^2}{s}\right)\,. \quad (2)$$

The last expression was obtained assuming a constant total cross section for $gg\to gg$ (i.e., the weak logarithmic energy dependence was neglected).

In order to reproduce the observed elliptic flow for the light-parton background at RHIC, scattering cross sections between light partons were scaled by a common factor to obtain $\sigma_{gg\to gg}=45\,\mathrm{mb}$ [23, 24], about fifteen times the elastic $2\to2$ perturbative QCD estimate. This value then fixes the total cross sections for all light-parton channels. On the other hand, in the spirit of a recent study based on Fokker–Planck dynamics [28], the enhancement of heavy-quark cross sections was considered to be a free parameter. The motivation for this is that these phenomenological factors (in part) attempt to incorporate the effect of radiative processes, which are more important for light partons than for the more slowly moving heavy quarks.

The parton initial conditions for Au + Au at $\sqrt{s_{NN}}=200\,\mathrm{A\,GeV}$ at RHIC were similar to those in [36], except that both initial charm and bottom production was, of course, included. For light partons, leading-order pQCD minijet three-momentum distributions were used (with a K-factor of 2, GRV98LO PDFs, and $Q^2{=}p_\mathrm{T}^2$, while $Q^2=\hat{s}$ for charm). The low-p_T divergence in the jet cross sections was regulated via a smooth extrapolation below $p_\perp<2\,\mathrm{GeV}$ to yield a total parton $\mathrm{d}N(b{=}0)/\mathrm{d}y=1000$ at midrapidity. This choice is motivated by the observed $\mathrm{d}N_\mathrm{ch}/\mathrm{d}y\sim700$ and the idea of local parton–hadron duality [42]. More novel hadronization mechanisms, such as parton coalescence, would imply quite different initial conditions [43, 44]. Heavy quark momentum distributions were taken from the fixed-order plus next-to-leading-log (FONLL) calculation in [45], except for the charm–anticharm correlation results in Sect. 3.4 for which correlated c–$\bar{c}$ distributions were obtained using the PYTHIA event generator [46]. The transverse density distribution was proportional to the binary collision distribution for two Woods–Saxon distributions; therefore $\mathrm{d}N^\mathrm{parton}(b{=}8\,\mathrm{fm})/\mathrm{d}y\approx250$. Perfect $\eta=y$ correlation was assumed.

Because heavy quarks are very rare, scatterings between heavy quarks and also the feedback of heavy quarks on the light-parton background were neglected. The transport equation (1) then becomes *linear* in the heavy-quark phase-space distributions, allowing for *weighted* test particle sampling $f(\mathbf{x},\mathbf{p},t)=\sum_{i=1}^{N_\mathrm{test}} w_i\delta^3(\mathbf{x}-\mathbf{x}_i(t))\delta^3(\mathbf{p}-\mathbf{p}_i(t))$. The advantage is that sparse, high-p_T phase-space regions can be sampled better (the test particle density can be increased anywhere in phase space, provided the weight is reduced in inverse proportion).

3 Results for heavy flavor

This section contains heavy-flavor results from the transport model MPC [35], for conditions expected at RHIC. The results are labeled by the heavy-quark–gluon scattering cross section σ, for which a wide range was explored, from the leading-order perturbative QCD estimate of $\sigma\sim1.3\,\mathrm{mb}$ up to a 15 times enhanced value, $\sigma=20\,\mathrm{mb}$.

3.1 Nuclear suppression of charm and bottom

A common observable to characterize parton energy loss is the nuclear suppression factor

$$R_{AA}(p_{\mathrm{T}}) \equiv \frac{\text{measured yield in } A+A}{\text{expectation for indep. } N+N \text{ scatterings}} ,$$

which compares the yields to the hypothetical case of independent nucleon–nucleon scatterings. In this study, the only nuclear effect considered is partonic rescattering; therefore, the $N+N$ baseline is given by the initial momentum distributions.

Figure 1 shows charm and bottom R_{AA} at midrapidity as a function of p_{T} from covariant transport for Au+Au at $\sqrt{s_{NN}} = 200$ GeV, with impact parameter $b = 8$ fm. At high p_{T} values, $p_{\mathrm{T}} > 5$ GeV, heavy-quark yields are suppressed because of elastic $2 \to 2$ energy loss, and the suppression becomes stronger with increasing heavy-quark scattering cross section σ. At the same σ, bottom is less suppressed than charm, due to the larger bottom mass. Remarkably, already the perturbative $\sigma = 1.3$ mb generates a significant suppression $R_{AA} \approx 0.6$–0.7.

At low p_{T}, R_{AA} grows with decreasing p_{T} as a natural consequence of energy loss. For the largest $\sigma = 20$ mb, the charm R_{AA} develops a peak near $p_{\mathrm{T}} \approx 2$ GeV, which is a clear sign of collective flow (the final spectrum has a "shoulder-arm" shape due to radial boost). In addition, for such large cross sections, the midrapidity ($|y| < 1$) charm yield is significantly reduced by diffusion in rapidity, which is the reason why R_{AA} is below one at all p_{T}.

The charm suppression results are qualitatively similar to those from the Fokker–Planck approach in [28]. The main difference is that charm R_{AA} from the Fokker–Planck drops much faster as p_{T} increases and does not show any sign of charm diffusion in rapidity. This is likely because a large *final* p_{T} biases towards fewer scatterings; moreover, atypical ("lucky") scatterings contribute significantly to the high-p_{T} yield [47]. These effects reduce the validity of the Fokker–Planck approach at high p_{T}.

3.2 Elliptic flow of charm and bottom

In noncentral $A+A$ reactions, an independent measure of energy loss and deflections in multiple scatterings is differential "elliptic flow", $v_2(p_{\mathrm{T}}) \equiv \langle \cos(2\phi) \rangle_{p_{\mathrm{T}}}$, the second Fourier moment of the azimuthal distribution relative to the reaction plane at a given p_{T}. Figure 2 shows charm and bottom $v_2(p_{\mathrm{T}})$ results at midrapidity for Au+Au at $\sqrt{s_{NN}} = 200$ GeV with $b = 8$ fm from covariant transport. In the $0 < p_{\mathrm{T}} < 5$ GeV window studied, the results are consistent with a monotonic increase with p_{T} for both

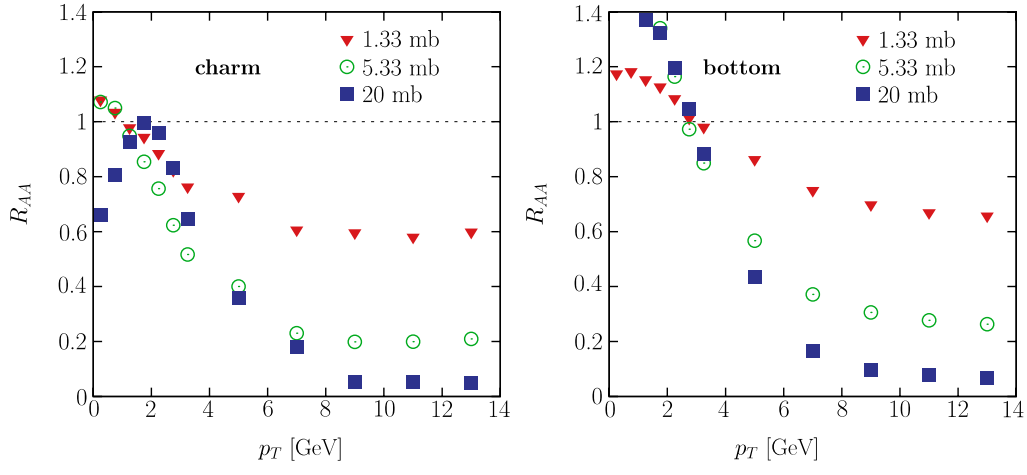

Fig. 1. Nuclear suppression factor R_{AA} for charm (*left*) and bottom quarks (*right*) as a function of p_{T} in Au+Au at $\sqrt{s_{NN}} = 200$ GeV with $b = 8$ fm, calculated using the covariant transport model MPC [35] with heavy-quark–gluon scattering cross sections $\sigma = 1.33$ (*triangles*), 5.33 (*open circles*), and 20 mb (*filled squares*)

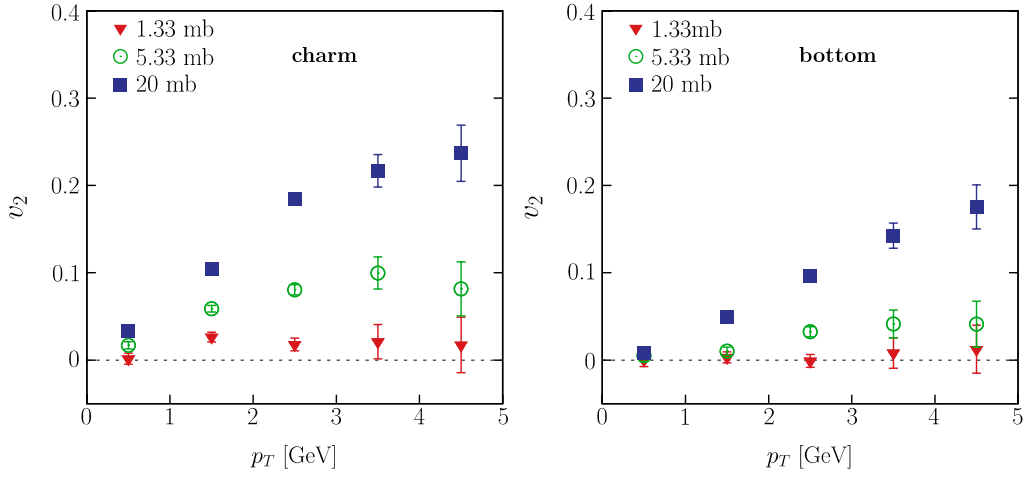

Fig. 2. Differential elliptic flow v_2 for charm (*left*) and bottom quarks (*right*) as a function of p_{T} in Au+Au at $\sqrt{s_{NN}} = 200$ GeV with $b = 8$ fm, calculated using the covariant transport model MPC [35] with heavy-quark–gluon scattering cross sections $\sigma = 1.33$ (*triangles*), 5.33 (*open circles*), and 20 mb (*filled squares*)

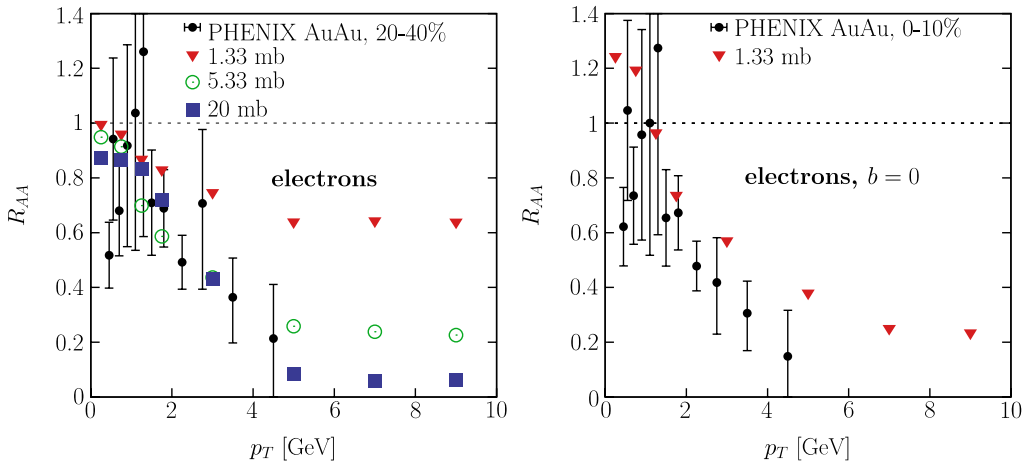

Fig. 3. *Left plot* shows nuclear suppression factor R_{AA} for decay electrons from charm and bottom as a function of p_T in Au + Au at $\sqrt{s_{NN}} = 200$ GeV with $b = 8$ fm, calculated using the covariant transport model MPC [35] with heavy-quark–gluon scattering cross sections $\sigma = 1.33$ (*triangles*), 5.33 (*open circles*), and 20 mb (*filled squares*). The *right plot* shows the same but for $b = 0$ fm and $\sigma = 1.33$ mb only. Data on "non-photonic electrons" from PHENIX [31, 32] (*filled circles*) with *statistical* errors are also shown

charm and bottom. For charm, the increase slows down above $p_T > 4$ GeV, indicating a turn-over at perhaps $p_T \sim$ 5–8 GeV. At the same p_T and σ, bottom v_2 is below charm v_2, as generally expected from the mass hierarchy [48] observed, in the lower mass region, $m \lesssim 1.5$ GeV, by earlier transport [29, 36] and ideal hydrodynamic calculations [12–15]. For the perturbative estimate $\sigma \sim 1.3$ mb, charm and bottom elliptic flow are very small, at most a few percent. Sizable heavy-quark elliptic flow $v_2 \sim 0.1$ at moderate $p_T \sim 2$–3 GeV requires 5–10 times enhanced cross sections.

The charm elliptic flow results agree well with earlier results from covariant transport [36] and also agree within a factor of 2 with results from the AMPT transport model [29]. The latter calculation considered *quark–quark* scattering with 3 mb and 10 mb cross sections (no gluons) and 2–3 times higher parton densities (constituent quarks from the "string melting" scenario), which is roughly equivalent to the opacities for $\sigma \sim 6$–8 and 20–25 mb in our case. Charm v_2 from AMPT tends to be lower and also saturates earlier, around $p_T \sim 2$ GeV, whereas our results continue to grow until $p_T \sim 3$–4 GeV. It would be important to investigate whether the discrepancy is due to differences in initial conditions, or the lack of covariance in the AMPT algorithm that has no parton subdivision.

The results compare qualitatively well to those from the Fokker–Planck approach in [28]. The main difference is that the Fokker–Planck v_2 has a higher slope at low p_T (i.e., much weaker "mass effect" for charm) and thus saturates earlier at high p_T. In addition, elliptic flow from the transport does not exhibit a peak (sharp "rise" and "drop") at moderate p_T, even for the largest cross section studied here.

3.3 Suppression and elliptic flow of decay electrons

Unfortunately, charm and bottom hadrons are difficult to reconstruct experimentally. Though various upgrades are underway to improve detection capabilities, the compromise at present is to look at "non-photonic" electrons, i.e., electrons (and positrons) coming, predominantly, from charm and bottom decays.

Figures 3 and 4 show decay electron results from the transport for Au + Au at $\sqrt{s_{NN}} = 200$ GeV. The electron (and positron) spectra were calculated via fragmenting the heavy quarks into D- and B-mesons, which were then decayed using the PYTHIA event generator [46]. Data from

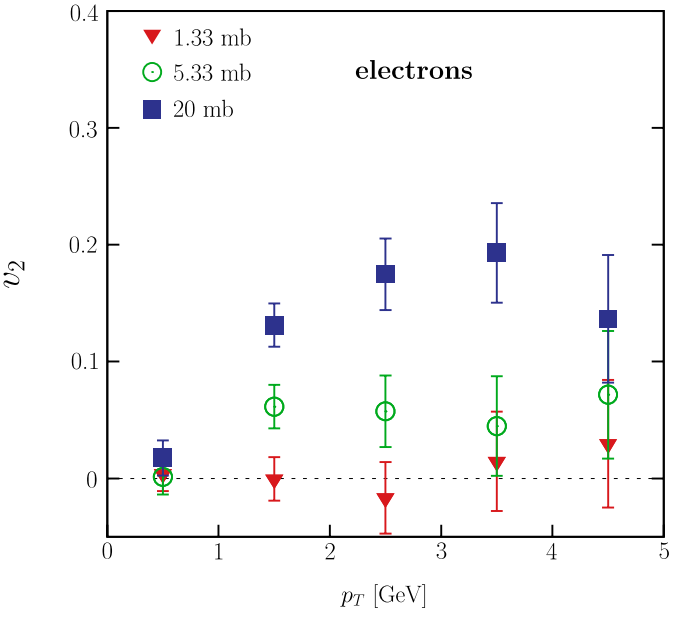

Fig. 4. Differential elliptic flow v_2 as a function of p_T for decay electrons from charm and bottom in Au + Au at $\sqrt{s_{NN}} =$ 200 GeV with $b = 8$ fm, calculated using the covariant transport model MPC [35] with heavy-quark–gluon scattering cross sections $\sigma = 1.33$ (*triangles*), 5.33 (*open circles*), and 20 mb (*filled squares*)

$d+$Au collisions at RHIC indicate a very hard heavy-quark fragmentation, dominated by momentum fractions $z \approx 1$ [49]. For simplicity, we therefore take fragmentation functions $F_{c\to D}(z) = \delta(1-z) = F_{b\to B}(z)$ and consider only $D^{\pm}$, D^0, $\bar{D}^0$ and the corresponding B-meson states.

At high $p_{\rm T}$, electron suppression is very similar in magnitude to that of heavy quarks, as can be seen in Fig. 3. The calculations for both $b = 0$ and 8 fm (about 30% centrality) indicate insufficient suppression for perturbative QCD rates. Though experimental uncertainties are large, one may speculate that a factor of ~ 5 or higher enhancement of the heavy-quark rates is needed for better agreement (a possible enhancement mechanism is discussed in [27]). At low $p_{\rm T}$, much of the structure seen in the heavy-quark R_{AA} (Fig. 1) gets washed out due to the decay kinematics.

Figure 4 shows the transport results for the elliptic flow of electrons (and positrons) from charm and bottom decays at midrapidity. Overall, the electron $v_2(p_{\rm T})$ is very similar to that of charm quarks, except shifted to somewhat lower $p_{\rm T}$ values (as expected from decays). This corroborates the findings in [50] that only considered electrons from charm decays. Compared to leading-order perturbative heavy-quark cross sections that give only a few percent elliptic flow, a significant $v_2 \sim 5$–10% from the transport requires a 4–8 times increase in heavy-quark scattering rates to $\sigma \sim 5$–10 mb. Based on the electron R_{AA} data, which suggest $\sigma \gtrsim 5$ mb, one expects an electron $v_2 \gtrsim 5\%$ at moderate $p_{\rm T} \sim 1.5$–5 GeV. Preliminary data by STAR [51] and PHENIX [52, 53] are compatible with an electron elliptic flow of this magnitude, but experimental uncertainties unfortunately prohibit an accurate cross-check.

For the largest $\sigma = 20$ mb from the transport, at the highest $p_{\rm T}$, $p_{\rm T} \approx 4$–5 GeV, the results show a decrease in electron elliptic flow. This is because bottom decay contributions to the overall electron yield start to become significant (eventually take over at higher $p_{\rm T}$), and bottom has a weaker elliptic flow (cf. Fig. 2).

3.4 Charm–anticharm azimuthal correlations

Rescatterings not only influence the suppression factor and elliptic flow but also the azimuthal correlations between two heavy quarks. Figure 5 shows the charm–anticharm correlation pattern expected for Au + Au at $\sqrt{s_{NN}} = 200$ GeV with $b = 8$ fm from covariant transport. In the calculation of this observable, the (correlated) initial charm distributions were taken from PYTHIA [46]. PYTHIA predicts a strong away-side peak in $N+N$ collisions (i.e., for $\sigma = 0$). However, the transport results show a correlation strength that is very sensitive to heavy-quark rescattering in heavy-ion collisions. The away-side peak is already reduced by about half for the small perturbative value $\sigma \approx 1.3$ mb, and as the cross section is increased further, the peak rapidly weakens and broadens. Eventually, for very large σ, the correlation changes character, and a very broad near-side peak appears. Measurements of charm–anticharm, such as the D-meson azimuthal correlations, can therefore provide an independent way to determine the effective heavy-quark scattering rates in the dense nuclear medium formed in heavy-ion collisions.

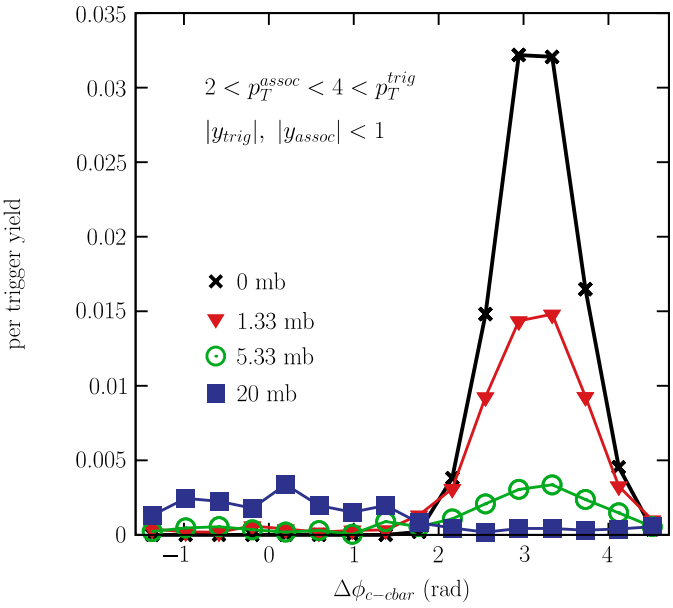

Fig. 5. Charm–anticharm azimuthal correlation in Au + Au at $\sqrt{s_{NN}} = 200$ GeV with $b = 8$ fm, calculated from the covariant transport model MPC [35] with heavy-quark–gluon scattering cross sections $\sigma = 1.33$ (*triangles*), 5.33 (*open circles*), and 20 mb (*filled squares*). Charm quarks/anti-quarks with $p_{\rm T} > 4$ GeV (*triggers*) were correlated with (associated) charm anti-quarks/quarks with $2 < p_{\rm T} < 4$ GeV. The correlation without charm rescatterings is also shown (*crosses*)

4 Conclusions

In this work we present heavy-flavor observables in Au + Au at RHIC (mainly for impact parameter $b = 8$ fm) from covariant parton transport theory. The heavy-quark phase-space evolution was studied in an order of magnitude more opaque light-parton (quark and gluon) system than a perturbative parton gas with leading-order $2 \to 2$ interactions [23, 24]. The calculation was driven by the cross section σ of heavy-quark interactions with gluons. The transport solutions were obtained using the covariant MPC algorithm [25, 35].

We find significant charm and bottom suppression with $R_{AA} \sim 0.5$–0.65 at high $p_{\rm T}$, $p_{\rm T} > 4$ GeV, already for leading-order heavy-quark matrix elements and a decreasing R_{AA} as the cross section increases (Fig. 1). Electrons from heavy-quark decays show a suppression pattern very similar in magnitude to that of the heavy quarks (Fig. 3). Consistency with data from RHIC [31–33] on "non-photonic" electrons requires a roughly five-fold increase in heavy-quark opacities relative to perturbative $2 \to 2$ scattering (more precise data would give better constraints).

The charm and bottom elliptic flow $v_2(p_{\rm T})$ from covariant transport is at most a few percent for the perturbative estimate of $\sigma \sim 1.3$ mb. Significant heavy-quark elliptic flow $v_2 \gtrsim 0.1$ at moderate $p_{\rm T} \sim 2$–3 GeV requires about five-fold or more enhanced heavy-quark rescattering (Fig. 3). The electron $v_2(p_{\rm T})$ is very similar to that of charm, at least up to $p_{\rm T} \approx 5$ GeV, where bottom contri-

butions to the decay electron yield start to become important. For heavy-quark opacities indicated by the non-photonic electron R_{AA} data at RHIC, the transport predicts $v_2 \sim 5$–10% (Fig. 4). This is within the large uncertainties of current measurements by STAR [51] and PHENIX [52, 53] – more accurate data are highly desirable.

In addition, we propose a unique observable, charm–anticharm azimuthal correlations, as an independent, sensitive probe of the degree of charm rescatterings in the dense parton medium (Fig. 5). High-$p_{\rm T}$, $p_{\rm T} > 4\,{\rm GeV}$ charm/anti-charm quarks (triggers) were correlated with moderate-$p_{\rm T}$, $2 < p_{\rm T} < 4\,{\rm GeV}$, anticharm/charm quarks, both at midrapidity. The strong away-side correlation peak in this observable predicted by PYTHIA for $N+N$ collisions is strongly reduced (and also broadened) due to rescatterings, by already a factor of two for the small perturbative cross section $\sigma \sim 1.3\,{\rm mb}$. At very large cross sections, the correlation pattern even changes to a broad near-side peak.

We emphasize that this study is limited to $2 \to 2$ transport. Contributions from radiative channels are likely important and should be included in the future. The results, nevertheless, can serve as a baseline calculation of elastic energy loss effects.

Finally, it would be interesting to extend this calculation with hidden heavy-flavor observables, such as J/ψ suppression, for which data are also available from RHIC.

Acknowledgements. We thank RIKEN, Brookhaven National Laboratory and the US Department of Energy [DE-AC02-98CH10886] for providing facilities essential for the completion of this work.

References

1. STAR Collaboration, C. Adler et al., Phys. Rev. Lett. **90**, 032 301 (2003)
2. STAR Collaboration, C. Adler et al., Phys. Rev. Lett. **87**, 182 301 (2001)
3. PHENIX Collaboration, K. Adcox, Phys. Rev. Lett. **89**, 212 301 (2002)
4. PHENIX Collaboration, K. Adcox et al., Phys. Rev. Lett. **88**, 022 301 (2002)
5. PHENIX Collaboration, S.S. Adler et al., Phys. Rev. Lett. **91**, 072 301 (2003)
6. STAR Collaboration, C. Adler et al., Phys. Rev. Lett. **89**, 202 301 (2002)
7. STAR Collaboration, J. Adams et al., Phys. Rev. Lett. **91**, 172 302 (2003)
8. M. Gyulassy, L. McLerran, Nucl. Phys. A **750**, 30 (2005)
9. H. Stoecker, Nucl. Phys. A **750**, 121 (2005)
10. E.V. Shuryak, hep-ph/0405066
11. D. Molnar, P. Huovinen, Phys. Rev. Lett. **94**, 012 302 (2005)
12. P.F. Kolb, J. Sollfrank, U. Heinz, Phys. Rev. C **62**, 054 909 (2000)
13. P. Huovinen et al., Phys. Lett. B **503**, 58 (2001)
14. D. Teaney, J. Lauret, E.V. Shuryak, nucl-th/0110037
15. T. Hirano, K. Tsuda, Phys. Rev. C **66**, 054 905 (2002)
16. X. Wang, Phys. Rev. C **63**, 054 902 (2001)
17. M. Gyulassy, I. Vitev, X.N. Wang, Phys. Rev. Lett. **86**, 2537 (2001)
18. M. Gyulassy et al., Phys. Lett. B **526**, 301 (2002)
19. Y.L. Dokshitzer, D.E. Kharzeev, Phys. Lett. B **519**, 199 (2001)
20. M. Djordjevic, M. Gyulassy, Phys. Lett. B **560**, 37 (2003)
21. M. Djordjevic, nucl-th/0603066
22. B. Zhang, M. Gyulassy, C.M. Ko, Phys. Lett. B **455**, 45 (1999)
23. D. Molnar, M. Gyulassy, Nucl. Phys. A **697**, 495 (2002)
24. D. Molnar, M. Gyulassy, Nucl. Phys. A **703**, 893(E) (2002)
25. D. Molnar, M. Gyulassy, Phys. Rev. C **62**, 054 907 (2002)
26. P.B. Gossiaux, V. Guiho, J. Aichelin, J. Phys. G **31**, S1079 (2005)
27. H. van Hees, R. Rapp, Phys. Rev. C **71**, 034 907 (2005)
28. G.D. Moore, D. Teaney, Phys. Rev. C **71**, 064 904 (2005)
29. B. Zhang, L.W. Chen, C.M. Ko, Phys. Rev. C **72**, 024 906 (2005)
30. Z. Xu, C. Greiner, Phys. Rev. C **71**, 064 901 (2005) talk by Z. Xu at this Workshop
31. PHENIX Collaboration, S.S. Adler et al., Phys. Rev. Lett. **96**, 032 301 (2006)
32. PHENIX Collaboration, K. Adcox et al., Phys. Rev. Lett. **88**, 192 303 (2002)
33. STAR Collaboration, J. Bielcik, nucl-ex/0511005
34. S. Wicks et al., nucl-th/0512076
35. D. Molnar, MPC version 1.8.3. This parton cascade code can be downloaded from WWW at: http://www-cunuke.phys.columbia.edu/people/molnard
36. D. Molnar, J. Phys. G **31**, S421 (2005)
37. B. Zhang, Comput. Phys. Commun. **109**, 193 (1998)
38. D. Molnar, M. Gyulassy, Phys. Rev. Lett. **92**, 052 301 (2004)
39. D. Molnar, Nucl. Phys. A **661**, 236 (1999)
40. Y. Pang, RHIC 96 Summer Study, preprint CU-TP-815 (unpublished)
41. B.L. Combridge, Nucl. Phys. B **151**, 429 (1979)
42. K.J. Eskola, K. Kajantie, P.V. Ruuskanen, K. Tuominen, Nucl. Phys. B **570**, 379 (2000)
43. D. Molnar, S.A. Voloshin, Phys. Rev. Lett. **91**, 092 301 (2003)
44. D. Molnar, Acta Phys. Hung. A **22**, 271 (2005) [nucl-th/0406066]
45. R. Vogt, private communication; M. Cacciari, P. Nason, R. Vogt, Phys. Rev. Lett. **95**, 122 001 (2005)
46. T. Sjostrand, Comput. Phys. Commun. **82**, 74 (1994)
47. D. Molnar, nucl-th/0503051
48. D. Molnar, nucl-th/0408044
49. STAR Collaboration, A. Tai, J. Phys. G **30**, S809 (2004)
50. V. Greco, C.M. Ko, R. Rapp, Phys. Lett. B **595**, 202 (2004)
51. STAR Collaboration, F. Laue, J. Phys. G **31**, S1121 (2005)
52. S.A. Butsyk, nucl-ex/0510010
53. PHENIX Collaboration, S.S. Adler et al., Phys. Rev. Lett. **96**, 032 001 (2006)